The Astrophysical Journal, 786:129 (12pp), 2014 May 10 doi:10.1088/0004-637X/786/2/129


# DIFFUSE $\gamma$-RAY EMISSION FROM UNRESOLVED BL LAC OBJECTS

M. Di Mauro[1,2], F. Donato[1], G. Lamanna[3], D. A. Sanchez[3], and P. D. Serpico[2]
[1] Physics Department, Torino University, and Istituto Nazionale di Fisica Nucleare, Sezione di Torino, via Giuria 1, I-10125 Torino, Italy; mattia.dimauro@to.infn.it
[2] Laboratoire d' Annecy-le-Vieux de Physique Théorique (LAPTh), Univ. de Savoie, CNRS, B.P.110, Annecy-le-Vieux F-74941, France
[3] Laboratoire d' Annecy-le-Vieux de Physique des Particules (LAPP), Univ. de Savoie, CNRS/IN2P3, Annecy-le-Vieux F-74941, France
*Received 2013 November 29; accepted 2014 March 21; published 2014 April 24*

## ABSTRACT

Blazars, active galactic nuclei with a jet pointing toward the Earth, represent the most abundant class of high-energy extragalactic $\gamma$-ray sources. The subset of blazars known as BL Lac objects is on average closer to Earth (i.e., younger) and characterized by harder spectra at high energy than the whole sample. The fraction of BL Lacs that is too dim to be detected and resolved by current $\gamma$-ray telescopes is therefore expected to contribute to the high-energy isotropic diffuse $\gamma$-ray background (IGRB). The IGRB has been recently measured over a wide energy range by the Large Area Telescope (LAT) on board the *Gamma-ray Space Telescope* (*Fermi*). We present a new prediction of the diffuse $\gamma$-ray flux due to the unresolved BL Lac blazar population. The model is built upon the spectral energy distribution and the luminosity function derived from the fraction of BL Lacs detected (and spectrally characterized) in the $\gamma$-ray energy range. We focus our attention on the $\mathcal{O}(100)$ GeV energy range, predicting the emission up to the TeV scale and taking into account the absorption on the extragalactic background light. In order to better shape the BL Lac spectral energy distribution, we combine the *Fermi*-LAT data with Imaging Atmospheric Cerenkov Telescope measurements of the most energetic sources. Our analysis is carried on separately for low- and intermediate-synchrotron-peaked BL Lacs on the one hand and high-synchrotron-peaked BL Lacs on the other hand: we find in fact statistically different features for the two. The diffuse emission from the sum of both BL Lac classes increases from about 10% of the measured IGRB at 100 MeV to ∼100% of the data level at 100 GeV. At energies greater than 100 GeV, our predictions naturally explain the IGRB data, accommodating their softening with increasing energy. Uncertainties are estimated to be within of a factor of two of the best-fit flux up to 500 GeV.

*Key words:* BL Lacertae objects: general – galaxies: active – galaxies: luminosity function, mass function – gamma rays: diffuse background – gamma rays: galaxies

*Online-only material:* color figures

## 1. INTRODUCTION

The origin of the observed isotropic diffuse $\gamma$-ray background (IGRB) at MeV–GeV energies is one of the most intriguing problems in astrophysics. The presence of an isotropic component was first suggested by the *OSO-3* satellite (Kraushaar et al. 1972) and then confirmed by *SAS-2* (Fichtel et al. 1975) and EGRET (Sreekumar et al. 1998). The *Fermi*-Large Area Telescope (LAT) has provided a measurement of this isotropic component showing that it can be adequately described as a single power law with an index of $-2.41 \pm 0.05$ in the 200 MeV–100 GeV energy range (Abdo et al. 2010d). Recently the *Fermi*-LAT Collaboration has presented a new estimation of the IGRB, based on 44 months of data in the range 200 MeV–400 GeV: at energy $E \geqslant 100$ GeV, the data points fall systematically below the extrapolation of the low-energy power-law best fit (Ackermann 2012).[4] We underline that these data are preliminary and error bands include systematics from effective area uncertainty and cosmic-ray background subtraction but not from foreground model uncertainties.

In several models, a significant fraction of the IGRB is attributed to unresolved extragalactic $\gamma$-ray sources. Blazars, belonging to the large family of active galactic nuclei (AGNs), represent the most numerous identified source population in the EGRET (Hartman et al. 1999) and *Fermi*-LAT (Nolan et al. 2012) catalogs and are expected to produce a substantial fraction of the IGRB. Typical predictions for blazars contributions to the IGRB range from 20% to 30% (Chiang & Mukherjee 1998; Mücke & Pohl 2000; Narumoto & Totani 2006; Dermer 2007; Kneiske & Mannheim 2007; Abazajian et al. 2011; Inoue & Totani 2009) to 100% (Stecker & Salamon 1996; Stecker & Venters 2011; Neronov & Semikoz 2012). Recently, an analysis of the source-count distribution at flux levels[5] $F_{100} \geqslant 10^{-9}$ photons cm$^{-2}$ s$^{-1}$ estimated that the contribution of unresolved blazars to the IGRB is ∼16% in the 100 MeV–100 GeV band (Abdo et al. 2010e). Since the source-count distributions show a strong break at $F_{100} \geqslant 6 \times 10^{-8}$ photons cm$^{-2}$ s$^{-1}$, it was concluded that, extrapolating the source counts to zero flux, the maximum contribution would be ∼23% of the IGRB.

An accurate modeling of the blazar contribution to the IGRB requires a careful consideration of their phenomenological classification. The spectral energy distributions (SEDs) of blazars exhibit a bimodal structure with a low-energy component attributed to synchrotron emission, while the nature of the high-energy emission is still under debate (Dermer et al. 1992; Henri et al. 1993; Begelman et al. 1990; Schlickeiser 2003). Blazars are traditionally divided into flat-spectrum radio quasars (FSRQs) and BL Lacertae (BL Lac) objects according to the presence or absence of strong broad emission lines in their optical/UV spectrum, respectively (Angel & Stockman 1980; Urry & Padovani 1995). Extending a scheme proposed for BL Lacs (Padovani & Giommi 1995), all the blazars may as well be classified according to the value of the synchrotron-peak

[4] http://galprop.stanford.edu/download/talks/13.Fermi_symposium_Ackermann.pdf

[5] $F_{100}$ represents the flux integrated above a threshold energy of 100 MeV.

frequency $\nu_S$, defining low-synchrotron-peaked (LSP) blazars when the peak frequency is observed in the far-infrared (FIR) or IR band ($\nu_S < 10^{14}$ Hz), intermediate-synchrotron-peaked (ISP) blazars when $\nu_S$ is in the near-IR to ultraviolet (UV) frequencies ($10^{14}$ Hz $\leqslant \nu_S < 10^{15}$ Hz), or as high-synchrotron-peaked (HSP) blazars if the peak frequency is located in the UV band or higher energies ($\nu_S \geqslant 10^{15}$ Hz) (Abdo et al. 2010a). Almost all the FSRQs with an SED classification are classified as LSP (Ackermann et al. 2011).

Recently, Ajello et al. (2012) examined the properties of $\gamma$-ray-selected FSRQs using data from the *Fermi*-LAT instrument. This work relies on a sample of 186 FSRQs detected by *Fermi*-LAT at high significance and large Galactic latitude during the first year of operation (Abdo et al. 2010b) and has thus important consequences for our understanding of the origins of the IGRB. The SEDs of all FSRQs show some curvature, with a peak in the 10 MeV–10 GeV range followed by a decrease leading to undetectable fluxes at energies higher than ~30 GeV. Moreover, the study of the FSRQ luminosity function (LF) shows a redshift distribution peaked at a redshift $z \sim 1$, with the farthest sources found at redshift values ~3.1 and $\gamma$-ray luminosity $\sim 10^{50}$ erg s$^{-1}$ (Ackermann et al. 2011; Ajello et al. 2012). The modeled SED and LF lead to a predicted contribution of the FSRQs to the IGRB of ~10% in the 1 MeV–10 GeV band. This analysis is in good agreement with the results reported by Abdo et al. (2010e), except above 10 GeV, where the use of a simple power law for the FSRQ spectra proved inadequate. Due to their redshift distribution and the absorption of $\gamma$-rays by the extragalactic background light, FSRQs are expected to give a negligible contribution to the IGRB above 10 GeV.

BL Lac blazars show different features if compared with FSRQs, and they are thus expected to give a different contribution to the IGRB. Their redshift distribution peaks around $z \sim 0.2$ and extends up to $z \approx 1.5$, at significantly lower redshifts than FSRQs (Ackermann et al. 2011). Also, marked differences exist in the distributions of $\gamma$-ray luminosity $L_\gamma$ and of spectral index $\Gamma$. The $L_\gamma$ distributions range between $L_\gamma \in [10^{45}, 10^{49}]$ erg s$^{-1}$ and $L_\gamma \in [10^{44}, 10^{47}]$ erg s$^{-1}$ for FSRQs and BL Lacs, respectively, while the corresponding $\Gamma$ distributions peak at $2.42 \pm 0.17$ for FSRQs, and it splits into $2.17 \pm 0.12$, $2.13 \pm 0.14$, and $1.90 \pm 0.17$ for LSP, ISP, and HSP, respectively (Ackermann et al. 2011). An immediate consequence of both the distance distribution (nearer for BL Lacs) and the spectral characteristics (harder for BL Lacs) is that the BL Lac contribution to the IGRB should be dominant above tens of GeV with respect to the FSRQ one. This is the region we concentrate on in the rest of this paper, even if we will provide our results on the diffuse emission from tens of MeV up to tens of TeV.

The IGRB well beyond tens of GeV (and up to sub-TeV energies) has been paid relatively minor attention in the past for a number of reasons. Most notably, it was a difficult range to access experimentally. This situation is changing thanks to the extended dynamical range and higher statistics of the *Fermi*-LAT instrument on one hand and to the improved performances of Imaging Atmospheric Cerenkov Telescopes (IACTs) on the other hand. Although IACTs are not particularly suitable for diffuse studies, the gradual lowering of energy thresholds and the increase of the collecting area (thanks to wide-dish telescopes) is allowing a more thorough exploration of the window of energy around $\mathcal{O}(100)$ GeV. Also, the greatly improved number of sources discovered in the TeV range allows us to meaningfully combine these data with *Fermi*-LAT results, leading to a more complete spectral characterization in the energy range of interest.

The aim of the paper is to predict the diffuse $\gamma$-ray emission from unresolved BL Lacs, in light of the currently available information. We consider a complete sample of BL Lacs detected during the first two years of *Fermi*-LAT operation to determine the LF, and we use *Fermi*-LAT data together with TeV data from the Cerenkov telescope, when available, to determine the SED. To our knowledge, this is the first time that such a synergic approach has been attempted. The article is structured as follows. Section 2 is devoted to the LF determination, Section 2.1 introduces the catalogs and the criteria used to select our sample, and Section 2.2 describes our fits to several models. Section 3 deals with the parameterization of the SEDs: similarly to the structure of the previous section, in subsection 3.1 we describe the data sets used, while subSection 3.2 details our fitting formulae and the results. Section 4 illustrates our prediction of the diffuse $\gamma$-ray emission from unresolved BL Lacs. Finally, Section 5 includes a discussion of the (astro)physical relevance of our findings, also comparing our results with diffuse $\gamma$-ray contributions from other unresolved sources, and presents some perspectives and conclusions. Some technical results concerning the fitting formulae of the LF and our HSP catalog are reported in Appendices A and B, respectively.

## 2. THE $\gamma$-RAY LUMINOSITY FUNCTION

### 2.1. The Catalog and Selection Cuts

For the determination of the $\gamma$-ray LF, we need the source distributions with respect to the redshift, the $\gamma$-ray luminosity, and an SED classification. We found that all the needed information can be obtained in the two-year *Fermi*-LAT Point Source Catalog (2FGL; Nolan et al. 2012), supplemented by two other catalogs (Shaw et al. 2012) for the determination of the redshift and the Second *Fermi* AGN Catalog (2LAC) for the SED classification (Ackermann et al. 2011) of the selected sources. As a whole, the 2FGL catalog contains 1873 sources, but for all the studies performed here we restrict ourselves to its subset of reliably detected, high-latitude objects, requirements that translate numerically into a galactic latitude $|b| > 10^\circ$ and value of the test statistics TS > 25 (corresponding to a significance larger than $\approx 5\sigma$ (Nolan et al. 2012)). These cuts select 1042 sources that effectively constitute our initial catalog, dubbed 2FGL*. We impose further selection criteria on this data set in order to determine the LF, as represented in Figure 1 and described below: in fact, the object classification, the distance distribution, and the $\gamma$-ray spectrum determination are all necessary ingredients in order to use the sample for our purposes.

First, we note that 169 out of the 1042 sources are unassociated. Among the associated sources, 357 are BL Lacs (and 318 FSRQs). Note that only 43% of the BL Lac objects have a measured redshift. Further, only 278 BL Lacs (78% of the total) have an SED classification (i.e., 79 sources cannot be classified owing to the lack of archival data), with HSPs representing the largest subclass (138 sources, 50% of SED-classified sources), ISPs the second largest (72 sources, 26%), and LSPs the smallest (68 sources, 24%). On the contrary, FSRQs with SED classification are 72% of the total and are essentially all LSPs (99%). Eventually, we end up with a catalog of 148 BL Lacs, divided into 34 LSP, 34 ISP, and 80 HSP objects.

The above-mentioned cut factors are, however, important in determining the incompleteness of the BL Lac sample, which

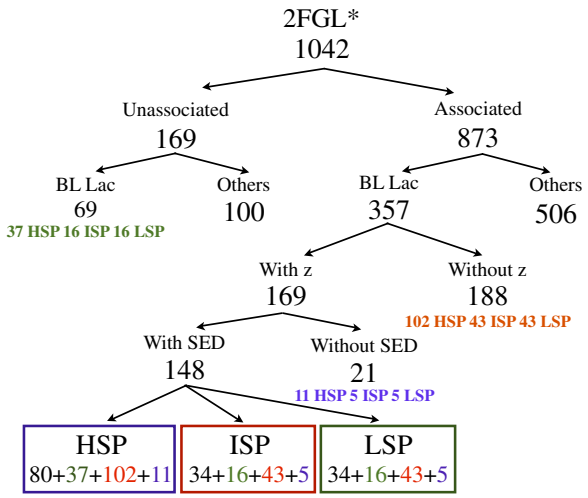


**Figure 1.** In this figure we sketch the source selection criteria we consider in our analysis for the calculation of the $\gamma$-ray LF. We list the steps bringing us from our initial catalog 2FGL* (namely, BL Lacs from 2FGL with $|b| > 10^{\circ}$ and TS $> 25$) to our final sample of sources; these are the independent requests of dealing with associated sources, with sources with measured redshift, and with sources with an SED classification. For each step we report also, with different colors, the number of BL Lacs that are discarded and have to be considered to infer the incompleteness factor of the sample (see text for details).

(A color version of this figure is available in the online journal.)

has to be corrected for this effect when inferring the properties of the whole population. The incompleteness of our sample is given by three independent factors:

1. *Unassociated sources.* The 2FGL* catalog contains 169 unassociated sources among the total of 1042 sources. This allows us to estimate the presence of further $169 \times 357/(1042–169) \approx 69$ BL Lacs among the unassociated sources, and in particular of about $69 \times 80/148 \approx 37$ HPSs, and $69 \times 34/148 \approx 16$ IPSs as well as LPSs. The inferred fraction of BL Lac objects in the unassociated sample is thus $\simeq$41%, which is compatible with the results derived in (Doert & Errando 2013). The relevant incompleteness factor is $(37 + 80)/80 \approx 1.46$ for HSP and $(16 + 34)/34 \approx 1.47$ for LSP and ISP objects.
2. *Lack of redshift.* For a total sample of 357 associated BL Lacs, only 169 have a measured redshift. Among the 188 sources without a redshift assignment, about 102 are HSP, and 43 are LSP as well as ISP BL Lacs. The lack of a measured value for the redshift gives an incompleteness factor of 2.28 for HSPs and 2.26 for LSPs and ISPs.
3. *Lack of SED.* We have considered only the BL Lacs with an SED classification. For a total sample of 169 BL Lacs with a measured redshift, only 148 have an SED classification. Among the 21 sources without an SED classification, about 11 are HSPs and 5 are LSPs and ISPs. The incompleteness factor associated with the lack of an SED classification is 1.14 for HSP and 1.15 for LSP and ISP BL Lacs.

The total incompleteness of the three subclasses can be thus estimated as $(80 + 11 + 102 + 37)/80 \approx 2.88$ for HSP and $(34 + 5 + 43 + 16)/34 \approx 2.88$ for LSP and ISP. We take into account these factors in the standard way (Ajello et al. 2012), namely, by correcting upward the normalization of the LF to reflect the inferred actual number of BL Lacs (associated or not, with or without a measured redshift and an SED classification). Note that due to the relatively small number of sources on which these correction factors have been estimated, a Poissonian uncertainty of $\mathcal{O}$(10%–20%) is typically associated with the average incompleteness factors reported above.

### 2.2. Fitting Models for the $\gamma$-Ray Luminosity Function

The characteristic parameters of an extragalactic source are the redshift $z$, the $\gamma$-ray luminosity $L_\gamma$, and the parameters describing the SED, notably the photon spectral index $\Gamma$. In the following section we demonstrate that the SED is better reproduced by a powerlaw with an exponential cutoff, so that at least one more parameter is needed. However, for the sake of notational simplicity, we shall omit an explicit mention of the cutoff energy parameter in the formulae in the remaining of this section. Additionally, in the energetic range 0.1–100 GeV that is used for the derivation of the LF, the $\gamma$-ray luminosity $L_\gamma$ and fluxes $F_{100}$ are not sensitive to the cutoff, and the spectral index $\Gamma$ actually constitutes the most important parameter. The space density of the BL Lac population may be expressed as

$$\Theta_\gamma(z, \Gamma, L_\gamma) = \frac{d^3N}{dz\, d\Gamma\, dL_\gamma} = \frac{d^2N}{dV\, dL_\gamma}\frac{dV}{dz}\frac{dN}{d\Gamma} = \rho_\gamma(z, L_\gamma)\frac{dV}{dz}\frac{dN}{d\Gamma}, \quad (1)$$

where $dV/dz$ is the co-moving volume element per unit redshift and unit solid angle (Hogg 1999) and $\rho(z, L_\gamma)$ is the LF defined as the number of sources per unit of comoving volume $V$ and luminosity $L_\gamma$(Willott et al. 2001):

$$\rho(z, L_\gamma) = \frac{d^2N}{dV\, dL_\gamma}. \quad (2)$$

The function $dN/d\Gamma$ is the (intrinsic) photon index distribution, assumed to be independent of the redshift, and, in analogy with Abdo et al. (2010e), Ajello et al. (2012), and Zeng et al. (2012), it is modeled as a Gaussian:

$$\frac{dN}{d\Gamma} = e^{\frac{(\Gamma-\mu)^2}{2\sigma^2}}, \quad (3)$$

where $\mu$ and $\sigma$ are the mean and the dispersion values of the Gaussian distribution, respectively, and will be fixed in the following to the best-fit values of the SED given in Table 1.

The aim of this section is to determine the space density of BL Lacs in Equation (1) as a function of the rest-frame energy 0.1–100 GeV luminosity ($L_\gamma$), the redshift ($z$), and the photon index ($\Gamma$), by comparing different predictions with the observed distributions of BL Lacs with respect to $L_\gamma$, $z$, as well as with the distribution of the number of sources with a flux higher than $F_\gamma$, $N(>F_\gamma)$. In order to describe the form of the LF in Equation (2), we considered the pure luminosity evolution (PLE; Hasinger et al. 2005a; Ueda et al. 2003), the luminosity-dependent density evolution (LDDE; Ueda et al. 2003), and the steep-spectrum radio source (SSRS; Willott et al. 2001) models. In the PLE model the redshift evolution is entirely in luminosity, while in the LDDE model the redshift evolution depends on the luminosity. These two models have been used in Ajello et al. (2012) to derive the $\gamma$-ray diffuse emission from FSRQs. On the other hand, the SSRS model has been deduced for SSRSs and has been employed by Inoue (2011), and Di Mauro et al. (2014) to find the diffuse $\gamma$-ray emission from misaligned AGNs. Further details and formulae are reported in the Appendix.

In order to find which of the three models is a better fit to our sample of BL Lac space density, we first build the experimental

**Table 1**
SED Best-fit Parameters

| | PWL | | LP | | | PLEC | | |
|---|---|---|---|---|---|---|---|---|
| | $\Gamma_{\rm pow}$ | $\tilde{\chi}^2$ (dof) | $\alpha$ | $\beta$ | $\tilde{\chi}^2$ (dof) | $\Gamma_{\rm cut}$ | $E_{\rm cut}$ (GeV) | $\tilde{\chi}^2$ (dof) |
| LSP | $2.18 \pm 0.12$ | 3.4 (114) | $2.13 \pm 0.13$ | $-1.05 \pm 0.30$ | 1.25 (113) | $2.08 \pm 0.13$ | $34^{+85}_{-20}$ | 0.80 (113) |
| ISP | $2.15 \pm 0.14$ | 2.6 (130) | $2.12 \pm 0.14$ | $-1.08 \pm 0.33$ | 1.10 (129) | $2.07 \pm 0.14$ | $39^{+80}_{-20}$ | 0.49 (129) |
| LISP | $2.17 \pm 0.15$ | 3.0 (246) | $2.13 \pm 0.15$ | $-1.06 \pm 0.33$ | 1.15 (245) | $2.08 \pm 0.15$ | $37^{+85}_{-20}$ | 0.63 (245) |
| HSP | $1.89 \pm 0.15$ | 5.4 (248) | $1.87 \pm 0.14$ | $-1.25 \pm 0.26$ | 1.34 (247) | $1.86 \pm 0.16$ | $910^{+1100}_{-450}$ | 0.48 (247) |

**Notes.** List of the best-fit values and uncertainties of the parameters for the SED of LSP, ISP, LISP, and HSP populations: the photon index $\Gamma_{\rm pow}$ of PWL, the $\alpha$ and $\beta$ parameters of the LP function, and $\Gamma_{\rm cut}$ and $E_{\rm cut}$ for PLEC. The corresponding values of the reduced chi-squared ($\tilde{\chi}^2$) and number of dof are also reported.

**Table 2**
Best-fit Parameters with $1\sigma$ Uncertainties for LDDE LF are Listed for LISP, HSP, and BL Lac together with the Value of the Reduced Chi-square $\tilde{\chi}^2$

| | $A$ ($10^{-9}$ Mpc$^{-3}$ erg$^{-1}$ s) | $L_c$ ($10^{48}$ erg s$^{-1}$) | $\gamma_1$ | $\gamma_2$ | $p_1$ | $p_2$ | $z_c^\star$ | $\alpha$ | $\tilde{\chi}^2$ (dof) |
|---|---|---|---|---|---|---|---|---|---|
| LISP | $4.37 \pm 0.78$ | $3.08 \pm 0.57$ | $1.19^{+0.26}_{-0.16}$ | $0.67^{+0.11}_{-0.16}$ | $4.4^{+2.1}_{-1.1}$ | $-2.9^{+1.3}_{-1.0}$ | $1.66^{+0.64}_{-0.49}$ | $0.36^{+0.15}_{-0.19}$ | 0.37 (32) |
| HSP | $98 \pm 18$ | $3.15 \pm 0.45$ | $2.88^{+1.32}_{-0.75}$ | $0.52^{+0.14}_{-0.17}$ | $-1.64^{+0.59}_{-0.56}$ | $4.8^{+1.4}_{-2.0}$ | $4.1^{+1.6}_{-2.2}$ | $0.25^{+0.11}_{-0.05}$ | 0.34 (30) |
| BL Lac | $96 \pm 13$ | $1.82 \pm 0.22$ | $0.59^{+0.15}_{-0.21}$ | $1.43^{+0.11}_{-0.08}$ | $1.54^{+0.86}_{-0.64}$ | $-0.42^{+0.23}_{-0.25}$ | $2.10^{+1.20}_{-1.25}$ | $0.052^{+0.030}_{-0.022}$ | 0.49 (39) |

$dN/dz$, $dN/dL_\gamma$, and $N(>F_\gamma)$ distributions from the following relations (Abdo et al. 2010e; Ajello et al. 2014):

$$\frac{dN}{dz} = \frac{1}{\Delta z}\frac{N_z}{\Delta\Omega}, \tag{4}$$

$$\frac{dN}{dL_\gamma} = \frac{1}{\Delta L_\gamma}\frac{N_{L_\gamma}}{\Delta\Omega}, \tag{5}$$

$$N(>F_\gamma) = \sum_{i=1}^{N_{F_\gamma}} \frac{1}{\Delta\Omega\,\omega(F_{\gamma,i})}, \tag{6}$$

where $\Delta z$ and $\Delta L_\gamma$ are the redshift and luminosity widths of the bin, $N_z$ and $N_{L_\gamma}$ are the numbers of BL Lacs counted in that bin of redshift or luminosity, and $\Delta\Omega$ is the solid angle ($|b| > 10^\circ$ in our case). The sum of Equation (6) is made for all the $i$th sources with a flux $F_{\gamma,i} > F_\gamma$. $\omega(F_{\gamma,i})$ is the *Fermi*-LAT efficiency at flux $F_{\gamma,i}$, and $N_{F_\gamma}$ is the number of the sources with a flux higher than $F_\gamma$. We use here the estimation of the efficiency $\omega(F_\gamma)$ derived in Di Mauro et al. (2014). For the above-cited experimental distributions we have taken into account the uncertainties associated with the finite number of sources in each bin $\propto\sqrt{N}$ (Poissonian uncertainties) and the uncertainty on the efficiency as in Ajello et al. (2012, 2014).

From Equation (1), the redshift, luminosity, and source-count distributions can be computed as (Ajello et al. 2012, 2014)

$$\frac{dN}{dz} = \int_{\Gamma_{\rm min}}^{\Gamma_{\rm max}} d\Gamma \int_{L_\gamma^{\rm min}}^{L_\gamma^{\rm max}} dL_\gamma\, \Theta_\gamma(z,\Gamma,L_\gamma)\,\omega(F_\gamma), \tag{7}$$

$$\frac{dN}{dL_\gamma} = \int_{\Gamma_{\rm min}}^{\Gamma_{\rm max}} d\Gamma \int_{z_{\rm min}}^{z_{\rm max}} dz\, \Theta_\gamma(z,\Gamma,L_\gamma)\,\omega(F_\gamma), \tag{8}$$

$$N(>F_\gamma) = \int_{\Gamma_{\rm min}}^{\Gamma_{\rm max}} d\Gamma \int_{z_{\rm min}}^{z_{\rm max}} dz \int_{L_\gamma(F_\gamma,z,\Gamma)}^{L_\gamma^{\rm max}} dL_\gamma\, \Theta_\gamma(z,\Gamma,L_\gamma), \tag{9}$$

where the limits of integration are $L_\gamma^{\rm min} = 10^{38}$ erg s$^{-1}$, $L_\gamma^{\rm max} = 10^{52}$ erg s$^{-1}$, $z_{\rm min} = 0$, $z_{\rm max} = 6$, $\Gamma_{\rm min} = 1.2$, and $\Gamma_{\rm max} = 3.0$ (we have checked that the results of the analysis have a negligible dependence on the limits of integration). $L_\gamma(F_\gamma, z, \Gamma)$ is the $\gamma$-ray luminosity for a source with a flux $F_\gamma$ in the range 100 MeV–100 GeV, a redshift $z$, and photon index $\Gamma$. The data on the redshift and $L_\gamma$ are less precise than the ones on the source-count distribution. On the other side, $dN/dz$ and $dN/dL_\gamma$ data are independent from each other, differently from the $N$ count data, which is a cumulative measure whose single data depends on all the ones at higher $F_\gamma$.

The fitting procedure consists of varying the values of the LF parameters and deducing, with the use of the MINUIT minimization package, the best-fit configuration with the relevant $1\sigma$ errors fitting the experimental number counts for the redshift, luminosity, and source distributions. We find that the reduced $\chi^2$ values are 0.49 for the LDDE model (39 degrees of freedom (dof)), 1.12 for the PLE model (41 dof), and 1.74 for the SSRS model (39 dof). The LDDE model turns out to be the best LF in reproducing the whole BL Lac population (similar results have been obtained very recently in Ajello et al. 2014). As will discussed in detail in Section 3.2, it is convenient to merge the LSP and ISP BL Lac classes into a unique population, which we will define LISP. We have therefore also fitted the different LF models separately for the two sub-classes represented by the LISP and HSP BL Lacs. The same results found for the whole sample hold true. The LDDE model is the preferred one, with reduced $\tilde{\chi}^2$ of 0.37 (32 dof) and 0.34 (30 dof) for LISP and HSP sources, respectively.

In Table 2 the best-fit parameters with $1\sigma$ uncertainties of the LDDE LF are listed for LISPs, HSPs, and the whole BL Lac population. In Figure 2 the theoretical and experimental redshift, luminosity, and source-count distributions are shown for LISPs, HSPs, and the BL Lac population as a whole, and assuming the LDDE LF model. The results in Figure 2 show that the HSPs have a narrow redshift distribution peaked around 0.1–0.2, while the LISPs have a broader distribution that extends to $z \approx 2$. Also, the $\gamma$-ray luminosity distribution is narrower for HSP than for LISP, with the latter class reaching values of $L_\gamma$ at least one order of magnitude higher. The source-count distribution shows that there are more high-flux LISPs than HSPs, while the opposite trend is present for low values of

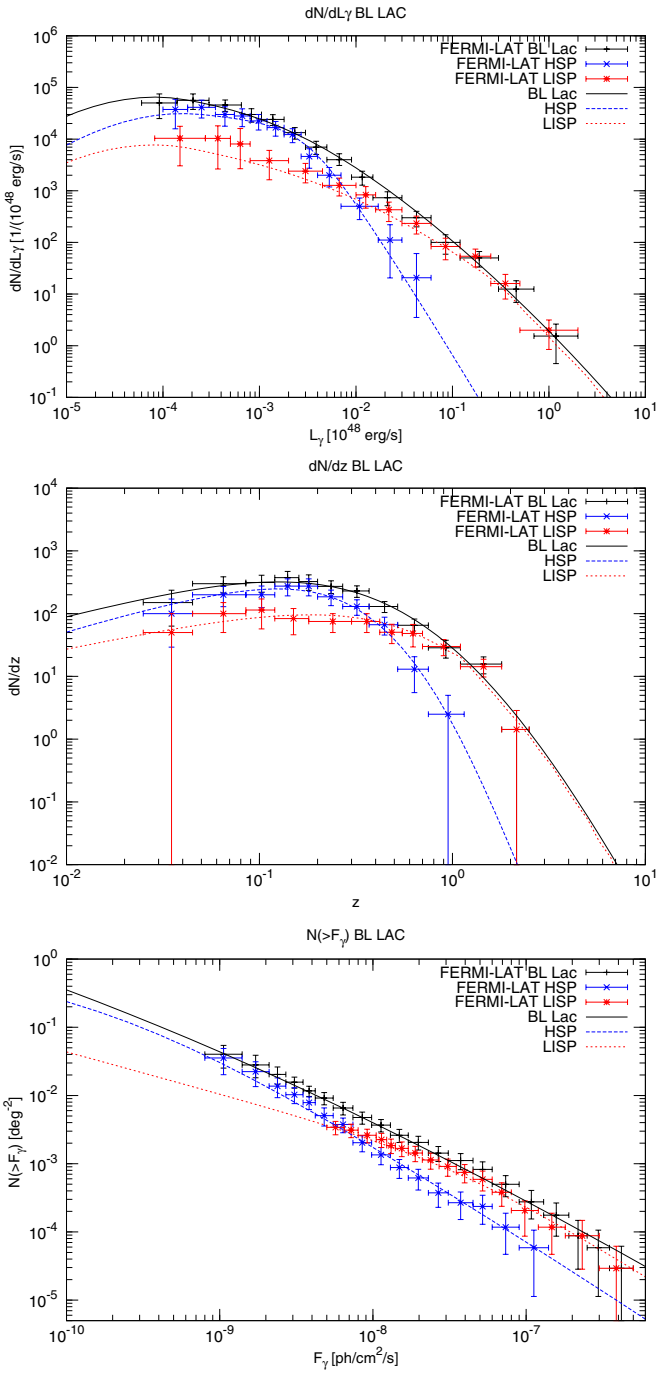


**Figure 2.** From top to bottom: theoretical and experimental luminosity, redshift, and source-count distributions are shown for LISPs (red dotted line/points), HSPs (blue dashed line/points), and for the whole (LISP+HSP) BL Lac sample (black solid line/points). Predictions are obtained with the LDDE LF model (Equation (A1)).

(A color version of this figure is available in the online journal.)

$F_\gamma$ (for $F_\gamma = 10^{-10}$ photons cm$^{-2}$ s$^{-1}$ the number of HSPs is about a factor of five higher than LISPs). The intensity of the diffuse $\gamma$-ray emission from unresolved BL Lac relies on the number of sources with a flux lower than the *Fermi*-LAT threshold ($\approx 10^{-9}$ photons cm$^{-2}$ s$^{-1}$). We expect, therefore, the bulk of the flux from unresolved BL Lacs to be due to HSPs, which are much more numerous than LISPs for very low $F_\gamma$.

## 3. PARAMETERIZATION OF THE SPECTRAL ENERGY DISTRIBUTIONS

### 3.1. The Catalog

For the SED parameterization, an implicit hypothesis for any population study is that some sort of spectral universality (or scaling with other independent parameters) is present in the sample, or at least in a selected sub-population. We take as template for this underlying spectrum the average SED inferred by fitting the single source data to some functional forms. Below we describe how these SEDs were obtained. Later on, we shall comment on the estimated systematic error intrinsic to our theoretical ansatz.

We are interested in obtaining a spectral fit of the three BL Lac sub-populations (LSP, ISP, HSP). However, one cannot simply take the spectra of the whole sample given by the 148 objects previously selected, since there is a known "spectral bias" to account for: *Fermi*-LAT more easily detects faint sources with a hard spectrum than those with a soft one[6] (Abdo et al. 2010c). To avoid this effect, we limit our spectral analysis to sources with $F_{100} > F_{100}^{\rm thr} = 1.5 \times 10^{-8}$ photons cm$^{-2}$ s$^{-1}$, which has been shown to ensure a detection efficiency independent of the photon index of the source (Ackermann et al. 2011).

After this further selection criterion on the catalog selected in Section 2.1, we are left with 19 LSP, 21 ISP, and 23 HSP BL Lacs, which we will employ for the averaged SED construction. A total of 57 sources out of the 63 in our sample are present in the First High Energy *Fermi*-LAT catalog (1FHL; The *Fermi*-LAT Collaboration 2013) based on 3 years of data. In this case, the highest energy point of the 2FGL was replaced in the fitting procedure by the data point of the 1FHL catalog. This ensures that one deals with statistically independent data points. Spectral information of the TeV emitters falling in the `default` section of the TeVCat catalog (Wakely & Deirdre 2013)[7] has also been added.

As expected, not all the objects detected at GeV scale have a TeV counterpart: on the contrary, most of the BL Lac objects in the current TeVCat are HSPs (41), while we found only 4 LSPs (with 3 FSRQs) and 7 ISPs. This confirms that the HSPs (sources with the highest value of the synchrotron-peak frequency) also have a high-energy component peaking from tens of GeV up to TeV energies (Abdo et al. 2010a; Boettcher 2012). Note also that among the 41 objects of the TeV catalog labeled as HSPs, 12 fall in the `newly announced` category, and their spectra are not publicly available. Among the remaining 29 objects, 7 are not present in the 2FGL catalog and are thus excluded in our study. Hence, our final sample of HSPs used to build the SED consists of 23 sources. It is important to note that, especially for the HSPs, the addition of the 1FHL and TeVCat catalogs—which are not used in the LF determination of Section 2.1—allows us to extend the energy range for the SED parameterization to the very high energy range.

Finally, we remind the reader that BL Lac objects are variable at all wavelengths. While flaring episodes in VHE were detected in the past (e.g., for Mrk 421 or PKS 2155−304), most of the sources do not show variability. This may be due to the fact that they were detected close to the sensitivity threshold with deep observations (several tens of hours) spread on few years. With the aim to reduce the possible bias introduced by the variability,

[6] Sources with $\Gamma = 1.5$ can be detected down to fluxes $\gtrsim$20 times fainter than those with a photon index of 3.0.

[7] http://tevcat.uchicago.edu

the lowest flux reported in the literature has been used based on Abdo et al. (2009), where the high and low flux states for flaring sources are reported. A similar procedure has been followed in Sanchez et al. (2013). A posteriori, a cross-check that this provides a reasonable approach is given by the goodness of fits with a single smooth function covering both the averaged/quiet-state *Fermi* spectrum at low energy and the spectrum at high energy from Cerenkov telescopes.

### 3.2. Spectral Energy Distribution Fits

The simplest model that can be tested to fit the SEDs is a power law (PWL):

$$\frac{dN}{dE} = K \left(\frac{E}{E_0}\right)^{-\Gamma_{\rm pow}}, \quad (10)$$

where $K$ is a normalization factor, $E_0$ is an arbitrary normalization energy, and $\Gamma_{\rm pow}$ is the photon spectral index. In the 2FGL catalog the spectra of AGNs are fitted with a lognormal parabola that is more general than the PWL. This shape is valid for bright sources (mainly AGNs), which are not very well represented by the power-law spectra. The lognormal (LP) function is given by

$$\frac{dN}{dE} = K' \left(\frac{E}{E_0}\right)^{-\alpha-\beta\log\left(\frac{E}{E_0}\right)}, \quad (11)$$

where $\alpha$ is the spectral slope at $E_0$ and $\beta$ is the curvature of the spectra. Finally, we also fit the data with a power law with an exponential cutoff (PLEC):

$$\frac{dN}{dE} = K'' \left(\frac{E}{E_0}\right)^{-\Gamma_{\rm cut}} \exp\left(-\frac{E}{E_{\rm cut}}\right), \quad (12)$$

where $E_{\rm cut}$ is the exponential cutoff energy and $\Gamma_{\rm cut}$ the power-law index associated with this spectral shape.

For HSPs, the data in the combined database (including 1FHL and TeVCat catalogs) extend up to the very high energy (VHE) range ($E \gtrsim 100$ GeV). At such energies, $\gamma$-rays from extragalactic sources have non-negligible probability to interact with extragalactic background light (EBL) photons. The intrinsic source spectrum $(dN/dE)_{\rm intr}$ is therefore modified because of the absorption of VHE $\gamma$-rays, and the observed spectrum $(dN/dE)_{\rm obs}$ reads

$$\left(\frac{dN}{dE}\right)_{\rm obs} = \left(\frac{dN}{dE}\right)_{\rm intr} \exp\left(-\tau_{\gamma\gamma}(E,z)\right), \quad (13)$$

where $\tau_{\gamma\gamma}(E,z)$ is the optical depth of the EBL. We adopt the model of Finke et al. (2010) for the EBL to correct the observed flux. This model is compatible with the recent EBL measurements provided by the *Fermi* and HESS Collaborations (Ackermann et al. 2012a; H.E.S.S. Collaboration et al. 2013a). We checked also for a sample of relevant redshifts that using the opacity of Franceschini et al. (2008) or Gilmore et al. (2012) would have a negligible impact on our results.

We fit the intrinsic spectra of our sample of HSPs, ISPs, and LSPs with the PWL, LP, and PLEC models. The best-fit values and the $1\sigma$ uncertainties on the best-fit parameters (apart from the normalization ones) for the SED of LSPs, ISPs, HSPs, and the entire BL Lac population are listed in Table 1. The corresponding values of the reduced chi-squared ($\tilde{\chi}^2$) and number of degrees of freedom are also reported. Note that the resulting values for the fitted photon index $\Gamma_{\rm pow}$ (PWL) are very close to the ones found in Ackermann et al. (2011), which reports $2.17 \pm 0.12$, $2.13 \pm 0.14$, and $1.90 \pm 0.17$ for LSP, ISP, and HSP, respectively.[8] On the other hand, using the PLEC model, the photon index $\Gamma_{\rm cut}$ is systematically harder than in the power-law fit case, especially for LSP and ISP. The HSPs also show systematically harder spectra (by more than 0.2 in the spectral index) and an inferred cutoff energy that is more than one order of magnitude higher than for either LSP or ISP objects.

For illustration, in the three panels of Figure 3 we show the SED for one representative source of each sub-class: an LSP object (top), an ISP object (middle), and an HSP object (bottom). We display the inferred intrinsic (EBL corrected) spectra (black points), together with the best-fit PWL, LP, and PLEC models for the intrinsic SED. Averaged best fit and the $1\sigma$ error band SED derived for each sub-class are also presented for comparison in the PLEC model.

Note that LSPs and ISPs have compatible values for the photon indices $\Gamma_{\rm pow}$, $\Gamma_{\rm cut}$ and the energy of the cutoff $E_{\rm cut}$. This is easily seen from the best-fit results, but can be quantified, for example, by performing a Student's $t$-test, which yields a compatibility of the two distributions of about 60%. We have therefore decided to merge the LSP and ISP populations into a unique class called LISP, with the following values (shown also in Table 1) for the photon index and energy cutoff: $\Gamma_{\rm pow} = 2.17 \pm 0.15$, $\Gamma_{\rm cut} = 2.08 \pm 0.15$, and $E_{\rm cut} = 37^{+85}_{-20}$ GeV. Additionally, we checked that the LISP and HSP populations are not compatible: a Student's $t$-test based on the power-law plus cutoff inferred parameter values yields a compatibility level well below 1%.

The chi-squared values for the different cases analyzed also show that a PLEC function provides the best description of the spectra of BL Lacs, among the ones tested (albeit other models like the PLE can still provide statistically acceptable fits). In general, we find that in several cases a mere power law is not a good description of VHE data. Note also that for LSP and ISP BL Lacs the average value of the photon index considering a simple power law is softer than the case of a power law with an exponential cutoff, confirming the presence of a turnoff in their spectra. On the contrary, in the case of HSPs the photon index values in the two cases are not so different, confirming that the cutoff occurs beyond the energy range explored by the LAT.[9]

Thus, in the following analysis we consider the BL Lac population split into two sub-classes: LISP with photon index $\Gamma_{\rm cut} = 2.08 \pm 0.15$ and energy cutoff $E_{\rm cut} = 37^{+85}_{-20}$ GeV, and HSP with photon index $\Gamma_{\rm cut} = 1.86 \pm 0.16$ and energy cutoff $E_{\rm cut} = 910^{+1100}_{-450}$ GeV. We show in Figure 4 the best fit and the uncertainty band for LISP and HSP BL Lac SEDs. The two spectra are normalized to $3 \times 10^{-12}$ erg cm$^{-2}$ s$^{-1}$ at 1 GeV. The uncertainty on the fitted SED is variable with energy. In particular, for the HSP sample it is about one order of magnitude at 100 MeV, a factor of three at 100 GeV, and it increases again at higher energies. For comparison, if we were to consider the BL Lac population globally with spectra given by a power law, we would obtain $\Gamma = 2.09 \pm 0.20$. Needless to say, a study based on such a simplifying assumption could provide a too crude representation of the data, especially in the highest energy range.

[8] No exact matching is expected, since our data set is enlarged compared with the one used in Ackermann et al. (2011).

[9] For a small number of sources (for HSP $\approx$ 20%), no statistically significant detection of a cutoff can be actually claimed; see also the discussion in Section 5.

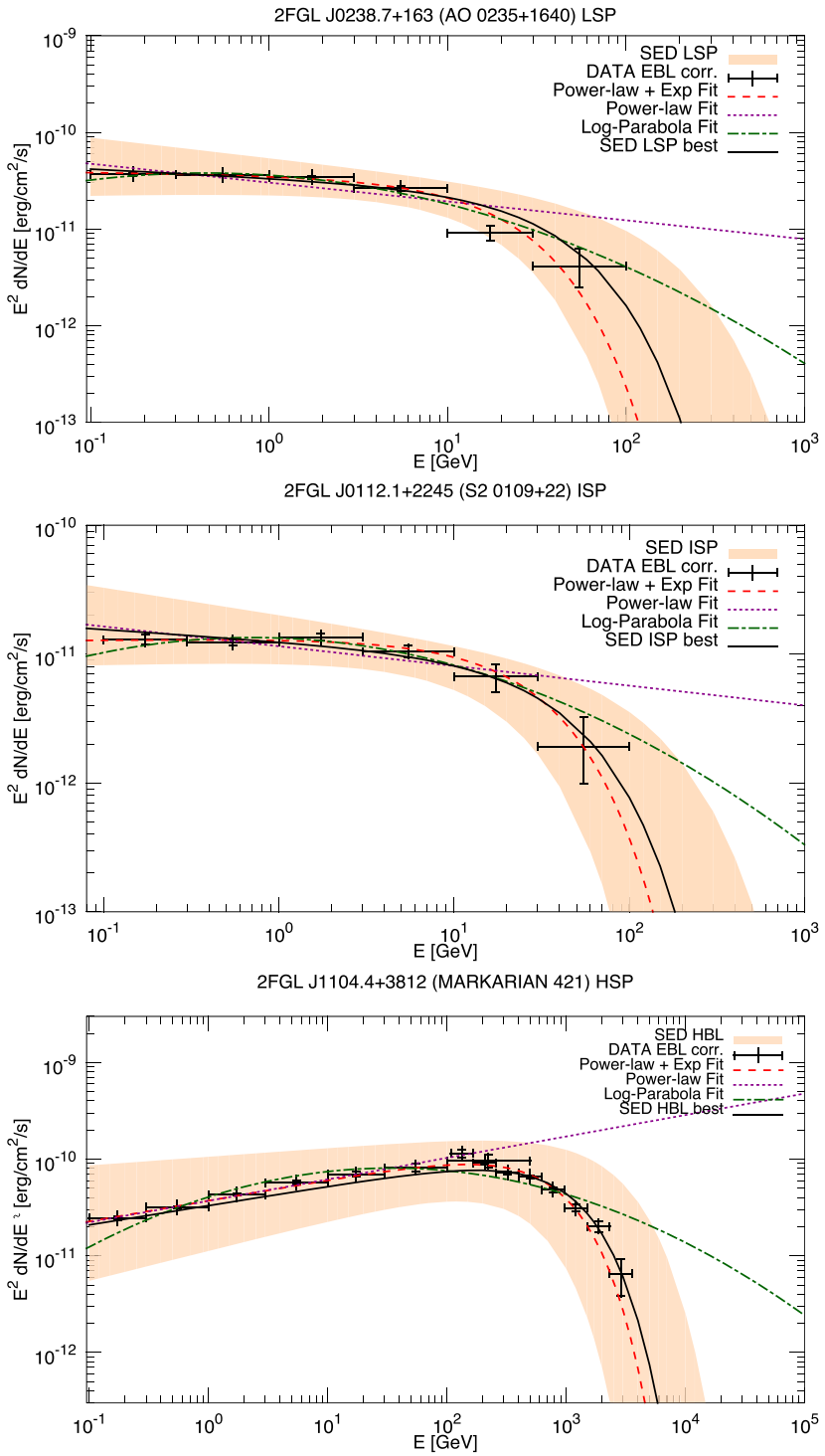


**Figure 3.** Top panel: SED of 2FGL J0238, an LSP in our sample. The points and curves represent the intrinsic derived spectrum (black points) and the theoretical SEDs computed from fitting the PWL (dotted purple line), LP (dot-dashed green line), and PLEC (dashed red line) functions with the intrinsic SED. We also display the best fit and the theoretical band (solid black line and pink band) of the SED derived for the LSP sample considering the PLEC model. Middle (bottom) panel: same as top panel, for 2FGL J0112 (Mrk 421), an ISP (HSP) in our sample.

(A color version of this figure is available in the online journal.)

Yet, in the following sections we shall see the usefulness of this model to gauge the systematic theory error on our predictions.

## 4. DIFFUSE $\gamma$-RAY EMISSION FROM UNRESOLVED BL LACS

Armed with the LF and SED previously derived, we are now ready to evaluate the $\gamma$-ray emission arising from faint BL Lacs. The contribution of unresolved BL Lacs to the IGRB can be estimated as

$$\Phi_{\rm IGRB}(E_\gamma) = \int_{\Gamma_{\rm min}}^{\Gamma_{\rm max}} d\Gamma \int_{z_{\rm min}}^{z_{\rm max}} dz \int_{L_\gamma^{\rm min}}^{L_\gamma^{\rm max}} dL_\gamma \, \Theta_\gamma(z, \Gamma, L_\gamma) \frac{dF_\gamma}{dE} \times e^{-\tau_{\gamma\gamma}(E,z)}[1 - \omega(F_\gamma)], \quad (14)$$

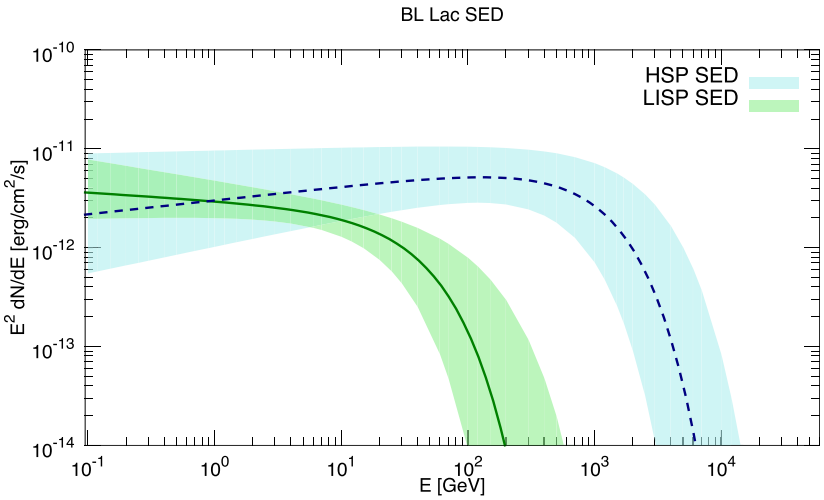


**Figure 4.** Best fit and uncertainty band obtained with the PLEC of the LISP (green) and HSP (cyan) BL Lac classes. The two spectra are normalized at $3 \times 10^{-12}$ erg cm$^{-1}$ s$^{-1}$ at 1 GeV, and they represent the intrinsic emission hence without the EBL absorption.

(A color version of this figure is available in the online journal.)

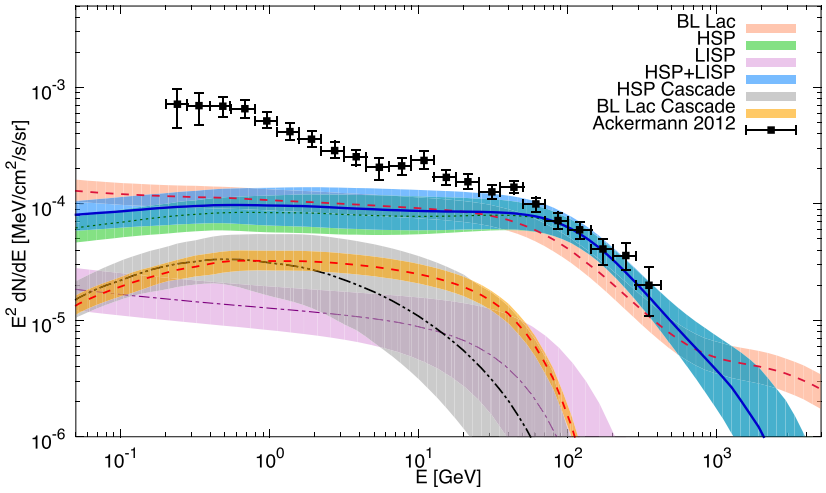


**Figure 5.** Diffuse $\gamma$-ray emission from unresolved BL Lacs. Predictions for the best-fit models (see text for details) are shown embedded in their $1\sigma$ uncertainty bands: the contribution is displayed for LISP (purple dot-dashed curve), HSP (dotted green), the sum of LISP and HSP (solid blue), and for BL Lacs considered as a unique population (dashed red). The IGRB data (Ackermann 2012) are also displayed with black points. The black dot-dashed (dashed yellow) line represents the cascade emission from the HSP (the whole BL Lac population) source flux.

(A color version of this figure is available in the online journal.)

where the limits of integrations are the same as reported in Section 2.2. $dF_\gamma/dE$ is the intrinsic photon flux at energy $E$, for a BL Lac with $\gamma$-ray luminosity $L_\gamma$ (Venters et al. 2009; Yan et al. 2012):

$$\frac{dF_\gamma}{dE} = \frac{L_\gamma\,(1+z)^{2-\Gamma}}{4\pi\, d_L(z)^2\, E_0^2}\,\mathcal{K}, \tag{15}$$

where $\mathcal{K}$ is a dimensionless spectral normalization factor (calculable numerically), which, for HSPs and in the limit $E_{\rm cut} \gg E_2, E_1$, is given by

$$\mathcal{K} \underset{E_{\rm cut} \gg E_2, E_1}{\longmapsto} \frac{(2-\Gamma)}{\left[\left(\frac{E_2}{E_0}\right)^{2-\Gamma} - \left(\frac{E_1}{E_0}\right)^{2-\Gamma}\right]}. \tag{16}$$

In the above formulae, $E_2 = 100$ GeV, $E_1 = 100$ MeV. The LAT detection efficiency function $(1-\omega(F_\gamma))$ (Di Mauro et al. 2014) enters in Equation (14) since we are interested in the diffuse flux not resolved by *Fermi*-LAT. Setting $\omega(F_\gamma) = 0$ allows us to compute the total $\gamma$-ray emission arising from the whole BL Lac class, either resolved or unresolved.

We use two different approaches to predict the flux from unresolved BL Lacs. Our best estimate is obtained considering the population as made by two sub-components, the LISP and the HSP BL Lacs, with the SEDs given by PLEC models. The second method assumes the BL Lac as a unique class of sources with an SED given by a simple power law. This (overly) simplistic model should provide an estimate of possible "systematic" biases coming from current misunderstanding of the BL Lac population, in particular in what concerns extrapolations to low fluxes or luminosities. We also calculate the uncertainty band for each case considering the $1\sigma$ errors on the LF and SED parameters for LISPs, HSPs, and BL Lacs given in Tables 1 and 2.

Our main results are reported in Figure 5, along with the *Fermi*-LAT IGRB data (Ackermann 2012). We present the predictions for the diffuse $\gamma$-ray emission from unresolved BL Lacs both when treated as a unique population and considering the two sub-populations of LISP and HSP separately. For the latter

case, the separate LISP and HSP contributions are displayed together with their sum. The high-energy LISP and HSP flux is shaped by the cutoff of the SEDs, while for the case of the BL Lacs treated as a unique population only the $\gamma$-ray EBL absorption intervenes in softening the spectrum (their SED being described by a simple power law) for energies $\gtrsim$30 GeV. Overall, the excellent agreement between our fiducial prediction (LISP+HSP) and the data suggests that unresolved HSP BL Lacs account for the largest fraction of the IGRB beyond about 50 GeV. Remarkably, Figure 5 indicates the even the simplistic/extreme model with a single population and power-law extrapolated SED would give a similar (albeit not as good) result in the energy decade around 100 GeV, although it overestimates the flux for the lowest energies and underestimates the flux at high energies. The EBL absorption alone can justify the measured decreasing trend in the IGRB spectrum above 100 GeV, albeit the shape suggested by the HSP SED (harder spectrum with exponential cutoff; see Section 3.2) seems to better reproduce the detailed trend.

The (very) high-energy radiation absorbed on the EBL via pair production may trigger a cascade photon production. The resulting $e^+e^-$ pairs, depending on the strength of the environmental magnetic fields, lose energy either via synchrotron radiation or via the inverse Compton process onto the cosmic microwave background (CMB). In the latter case, the up-scattered CMB photons end up typically at GeV energies and can contribute to the IGRB. We estimated this contribution using the formalism described, e.g., in Inoue & Ioka (2012) and applied to the mis-aligned AGN diffuse emission in Di Mauro et al. (2014), assuming that all the absorbed energy at VHE ends up in those re-scattered photons. We also set to zero the intergalactic magnetic field, which implies an upper limit for the cascade emission at the $\gamma$-ray energies. The results for the cascade photons are shown in Figure 5 with a gray (ochre) band for the HSP (BL Lac considered as a unique) population. This contribution amounts to no more than $\sim$30% of the primary flux, and additionally in the GeV range where the BL Lac contribution to the IGRB is anyway subdominant. It is worth nothing that the amount of this "tertiary" radiation depends on the amount of energy absorbed at VHE and hence on the hardness of the primary spectrum (the larger background expected at low energies for the baseline model follows from the HSP hard spectrum) and on the presence (and value) of an energy cutoff. Also note the larger dispersion of the prediction (especially at high energy) for the HSP case due to the strong impact of $E_{\rm cut}$. Despite its marginal role, the cascade contribution has been included in all the fluxes displayed in Figure 5.

## 5. DISCUSSION AND CONCLUSION

In this paper, we present a new calculation of the diffuse $\gamma$-ray emission expected from the unresolved BL Lac blazars. For the first time, we have focused attention on the $\mathcal{O}$(100) GeV energy range, pushing the predictions up to the TeV scale. To that purpose, while most of the statistical population properties rely on *Fermi*-LAT data, the synergy with IACT data has proven essential in modeling the spectrum of these objects at the energies of interest. The IACT data are fundamental in two respects: (a) in confirming that photons are indeed injected from BL Lacs up to the TeV energy, thus removing the ansatz of high-energy extrapolation; and (b) in refining the spectral shape determination. The HSP+LISP prediction in Figure 5 is clearly in good agreement with available data, within the estimated uncertainty band. Notably, our best estimation seems to *fully* account for the measured IGRB at $E_\gamma \gtrsim 50$ GeV: note that there is no free-parameter adjustment of prediction to data in Figure 5! Our detailed analysis thus confirms quantitatively the conjecture put forward in some earlier works as (Neronov & Semikoz 2012). Also, the role of BL Lacs is relatively subleading at low energies: for our fiducial best-fit model, the estimated contribution to the measured IGRB between 100 MeV and 100 GeV amounts merely to $\sim$11% of the *Fermi*-LAT data (in agreement with the results of Ajello et al. 2014).

Additionally, our analysis suggests that for (very) high energy $\gamma$-ray purposes it is meaningful to distinguish between HSP and the joint LSP and ISP (LISP) sub-classes. Considering HSP and LISP as a unique population would still lead to an acceptable prediction for the diffuse emission in the energy band considered, but at the expense of a relatively worse SED fit (see Table 1). The resulting prediction also falls a bit short of the measured IGRB, albeit the statistical significance of the difference is not high, yet. Also, the extrapolations to lower and higher energies are significantly different, potentially with implications for other aspects of $\gamma$-ray astrophysics.

Concerning the model uncertainties, we included in our predictions the $1\sigma$ errors coming from the LF and SED fits. A handle on the "systematic" theoretical uncertainties is notoriously more difficult to achieve. Yet, our exercise of using the oversimplified single population and power-law SED model leads to comparable results, strengthening our confidence in the predictions. Most likely, at least in the one decade around 100 GeV, the systematic errors are not larger than the statistical ones. Other causes of error are expected to be sub-leading: the "completeness function" $\omega$ is itself derived from data and is subject to some uncertainty. However, its impact on the unresolved flux is very modest (we estimate $\sim \mathcal{O}(5\%)$), since the factor $(1-\omega)$ entering in Equation (14) is very close to 1 at the low luminosities that contribute the most to the unresolved flux. Similarly, current observations by *Fermi*-LAT (Ackermann et al. 2012) or HESS (H.E.S.S. Collaboration et al. 2013a) corner quite well the range of opacities of the universe, at least at relatively low redshifts of major interest for our purpose. At TeV energies or beyond, however, more extreme assumptions on the level of EBL that may be still marginally allowed by the data could nonetheless affect our predictions by an amount comparable to the size of the error band shown in Figure 5. A more extensive study of those uncertainties may be justified, once IGRB data in that energy region will become available, and is left for future work.

Globally, the emerging picture seems to be that the IGRB may be naturally explained by the cumulative $\gamma$-ray emission from unresolved extragalactic (and, to some extent, galactic) sources, as already discussed in the Introduction. Needless to say, estimates exist in the literature for the contributions to the IGRB of other populations of unresolved astrophysical sources, such as FSRQs (Ajello et al. 2012), misaligned AGNs (Inoue 2011; Di Mauro et al. 2014), star-forming galaxies (Ackermann et al. 2012b), and galactic millisecond pulsars (Calore et al. 2012). Without the aim of completeness, it can be instructive to show in Figure 6 the unresolved $\gamma$-ray emission from the above-cited populations together with the one for BL Lacs computed in the present work. It is remarkable that the predicted best estimate (which is the sum of the best model for each population) is extremely close to the measured data points, which are found within the estimated uncertainty. This agreement extends over more than three decades of energy, suggesting that there is relatively little room for major extra sources of this diffuse

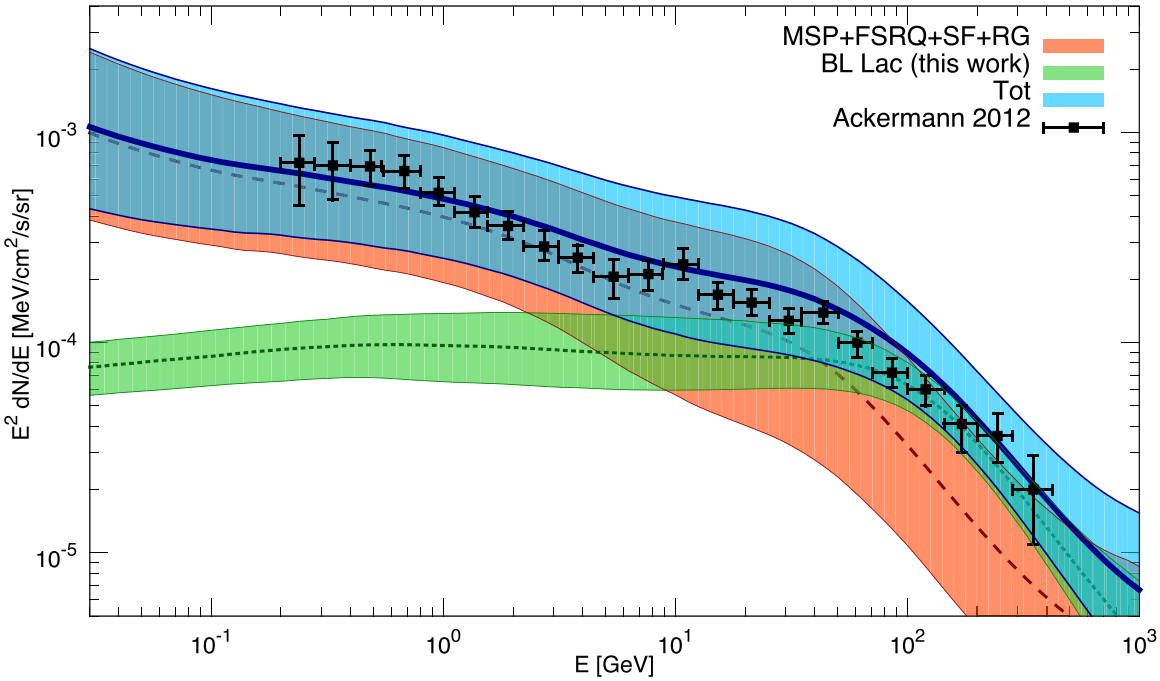


**Figure 6.** Global view of the diffuse $\gamma$-ray predictions (best-fit models and relevant uncertainty band) is displayed for unresolved BL Lacs (dotted green, this work) and for the sum of misaligned AGNs (Di Mauro et al. 2014), star-forming galaxies (Ackermann et al. 2012b), FSRQs (Ajello et al. 2012), and millisecond pulsars (Calore et al. 2012; orange dashed line and uncertainty band). IGRB data (Ackermann 2012) are also displayed with black points. The sum of all the predictions is displayed in a blue curve line and cyan uncertainty band.

(A color version of this figure is available in the online journal.)

background. The importance of strengthening these predictions in the future, via a consolidation a multi-messenger GeV–TeV cosmology thanks to instruments such as CTA (see, e.g., Reimer & Böttcher 2013; Dubus et al. 2013), should not be underestimated. In fact, apart from being a "sanity check" of our current understanding of *populations* of astrophysical accelerators, the IGRB has already been suggested to act as a diagnostic tool for subfields of astroparticle physics as diverse as ultra-high-energy cosmic rays (see, e.g., Kalashev et al. 2009) or indirect dark matter searches (as recently in Calore et al. 2012; Bringmann et al. 2013).

As an intriguing example, we note that for a minority (roughly 20%) of the HSP sources in our sample, the fitting procedure did not find any indication of cutoff in the spectra. This feature could be just an artifact of the limited sensitivity at high energies, or might hint to the existence of a new sub-class of sources (sometimes dubbed ultra-high-frequency-peaked BL Lac; Ghisellini 1999; Sentürk et al. 2013). In such a case, some departure from the baseline flux prediction presented in Figures 5 and 6 could most easily show up at TeV energies.

In this context, it is worth commenting on the fact that in recent years several authors have studied an alternative mechanism for generating hard TeV spectra from distant BL Lacs: line-of-sight interactions of cosmic rays ("protons") with cosmic microwave background radiation and EBL can generate secondary gamma rays relatively close to the observer and with hard spectra (see, e.g., Essey & Kusenko 2010; Murase et al. 2012; Prosekin et al. 2012; Zheng & Kang 2013). This is certainly an example of a scenario in which both the SED at VHE (even harder spectra, much higher cutoff energy, ...) and the LF (e.g., relatively large detectable population at large $z$) could depart from the minimal, two main population scenario discussed above. Interestingly, this would also open up a different diagnostic tool of gamma *propagation*, since cascades are much more sensitive to "environmental" parameters such as the EBL and the extra-galactic magnetic fields. Fortunately, it has been argued that future surveys have the potential to uncover these populations (see, e.g., Inoue et al. (2013)). No doubt, the next decade in VHE gamma astrophysics may still reserve some surprises!

We thank M. Ajello and L. Latronico for useful discussions. At LAPTh and LAPP, this activity was supported by the Labex grant ENIGMASS. F.D. further acknowledges support from AAP-"LeSAdHE" of University of Savoie.

## APPENDIX A

## MODEL PARAMETERIZATION TESTED FOR THE LF FITS

We have tested several models to fit the LF, notably the pure luminosity evolution (PLE), the luminosity-dependent density evolution (LDDE), and the steep-spectrum radio source (SSRS) models. For the sake of completeness, we report here their parameterizations.

Our best fit is obtained for the LDDE model (Ueda et al. 2003), in which the evolution is primarily in density, with a luminosity-dependent redshift peak. Its parameterization is

$$\rho(z, L_\gamma) = \rho(L_\gamma)\, e(z, L_\gamma), \tag{A1}$$

with

$$\rho(L_\gamma) = \frac{A}{\log(10) L_\gamma} \left[ \left( \frac{L_\gamma}{L_c} \right)^{\gamma_1} + \left( \frac{L_\gamma}{L_c} \right)^{\gamma_2} \right], \tag{A2}$$

$$e(z, L_\gamma) = \left[ \left( \frac{1+z}{1+z_c(L_\gamma)} \right)^{p_1} + \left( \frac{1+z}{1+z_c(L_\gamma)} \right)^{p_2} \right], \tag{A3}$$

**Table 3**
List of the Parameters for the Sample of 23 HSP BL Lacs Selected for the Determination of the SED

| Name | 2FGL Name | z | $\Gamma_{\rm HE}$ | $\Gamma_{\rm VHE}$ | $\Gamma_{\rm cut}$ | $E_{\rm cut}$ (GeV) |
|---|---|---|---|---|---|---|
| RGB J0152+017 | J0152.6+0148 | 0.080 | $1.79 \pm 0.14$ | $2.95 \pm 0.41$ | $1.82 \pm 0.13$ | $1970^{3300}_{1200}$ |
| RBS 0413 | J0319.6+1849 | 0.190 | $1.55 \pm 0.11$ | $3.18 \pm 0.74$ | $1.75 \pm 0.12$ | $630^{540}_{290}$ |
| 1ES 0414+009 | J0416.8+0105 | 0.287 | $1.98 \pm 0.16$ | $3.45 \pm 0.32$ | $1.83 \pm 0.04$ | // |
| PKS 0447−439 | J0449.4−4350 | $0.25 \pm 0.10$ | $1.86 \pm 0.02$ | $3.89 \pm 0.43$ | $1.88 \pm 0.02$ | $370^{240}_{75}$ |
| VER J0648+152 | J0648.9+1516 | 0.179 | $1.74 \pm 0.11$ | $4.4 \pm 0.9$ | $1.94 \pm 0.26$ | $450^{510}_{230}$ |
| RGB J0710+591 | J0710.5+5908 | 0.125 | $1.53 \pm 0.12$ | $2.69 \pm 0.33$ | $1.67 \pm 0.07$ | $2760^{2100}_{1100}$ |
| 1ES 0806+524 | J0809.8+5218 | 0.138 | $1.94 \pm 0.06$ | $3.6 \pm 1.0$ | $1.86 \pm 0.05$ | $510^{230}_{160}$ |
| 1ES 1011+496 | J1015.1+4925 | 0.212 | $1.72 \pm 0.04$ | $4.0 \pm 0.5$ | $1.84 \pm 0.02$ | $355^{190}_{120}$ |
| 1ES 1101−232 | J1103.4−2330 | 0.186 | $1.80 \pm 0.21$ | $2.94 \pm 0.20$ | $1.83 \pm 0.25$ | // |
| Markarian 421 | J1104.4+3812 | 0.031 | $1.77 \pm 0.01$ | $2.20 \pm 0.08$ | $1.785 \pm 0.006$ | $692^{34}_{32}$ |
| Markarian 180 | J1136.7+7009 | 0.045 | $1.74 \pm 0.08$ | $3.25 \pm 0.66$ | $1.75 \pm 0.07$ | $905^{570}_{350}$ |
| 1ES 1215+303 | J1217.8+3006 | 0.13 | $2.02 \pm 0.04$ | $2.96 \pm 0.21$ | $2.15 \pm 0.03$ | $2000^{2200}_{1040}$ |
| 1ES 1218+304 | J1221.3+3010 | 0.182 | $1.71 \pm 0.07$ | $3.08 \pm 0.39$ | $1.78 \pm 0.06$ | $1010^{1040}_{510}$ |
| H 1426+428 | J1428.6+4240 | 0.129 | $1.32 \pm 0.12$ | $3.5 \pm 0.35$ | $1.05 \pm 0.16$ | $570^{190}_{140}$ |
| PG 1553+113 | J1555.7+1111 | [0.43, 0.58] | $1.67 \pm 0.02$ | $4.5 \pm 0.3$ | $1.771 \pm 0.016$ | // |
| Markarian 501 | J1653.9+3945 | 0.034 | $1.74 \pm 0.03$ | $2.72 \pm 0.18$ | $1.835 \pm 0.014$ | $1630^{350}_{280}$ |
| 1ES 1959+650 | J2000.0+6509 | 0.048 | $1.94 \pm 0.03$ | $2.58 \pm 0.18$ | $1.98 \pm 0.02$ | $2750^{1600}_{1020}$ |
| PKS 2005−489 | J2009.5−4850 | 0.071 | $1.78 \pm 0.05$ | $3.20 \pm 0.19$ | $1.77 \pm 0.04$ | $220^{32}_{28}$ |
| PKS 2155−304 | J2158.8−3013 | 0.116 | $1.84 \pm 0.02$ | $3.32 \pm 0.06$ | $1.864 \pm 0.011$ | $350^{30}_{25}$ |
| B3 2247+381 | J2250.0+3825 | 0.119 | $1.84 \pm 0.11$ | $3.2 \pm 0.7$ | $1.77 \pm 0.13$ | // |
| 1ES 2344+514 | J2347.0+5142 | 0.044 | $1.72 \pm 0.08$ | $2.95 \pm 0.23$ | $1.71 \pm 0.07$ | $630^{170}_{130}$ |
| H 2356−309 | J2359.0−3037 | 0.165 | $1.89 \pm 0.17$ | $3.09 \pm 0.26$ | $1.71 \pm 0.11$ | $3720^{4700}_{2100}$ |

**Notes.** Columns: Name, 2FGL name, redshift, *Fermi*-LAT photon index from 100 MeV to 100 GeV $\Gamma_{\rm HE}$, VHE photon index measured at TeV energies by Cerenkov experiments $\Gamma_{\rm VHE}$, and photon index $\Gamma_{\rm cut}$ and energy cutoff $E_{\rm cut}$, both fitted in our Analysis according to Equation (12). The values associated with $\Gamma_{\rm HE}$, $\Gamma_{\rm VHE}$, and $z$ are taken from (Sanchez et al. 2013) for all sources except for 1ES 1215+303 (Aleksić et al. 2012), PKS 0447−439 (Perlman et al. 1998; Prandini et al. 2012; Rovero et al. 2013; Zhou et al. 2013; H.E.S.S. Collaboration et al. 2013b), PG 1553+113 (Danforth et al. 2010; Aharonian et al. 2008), and Mrk 501 (Acciari et al. 2011).

and

$$z_c(L_\gamma) = z_c^\star \left(\frac{L_\gamma}{10^{48}\ \mathrm{erg\ s^{-1}}}\right)^\alpha. \quad \text{(A4)}$$

The best-fit parameters and $1\sigma$ uncertainties for this model are reported in Table 2.

The PLE model (Ueda et al. 2003; Hasinger et al. 2005b) is given by the following parameterization:

$$\rho(z, L_\gamma) = \rho(L_\gamma / e(z)), \quad \text{(A5)}$$

where

$$\rho(L_\gamma/e(z=0)) = \frac{dN}{dL_\gamma} = \frac{A}{\log(10) L_\gamma}\left[\left(\frac{L_\gamma}{L_c}\right)^{\gamma_1} + \left(\frac{L_\gamma}{L_c}\right)^{\gamma_2}\right], \quad \text{(A6)}$$

and

$$e(z) = (1+z)^k e^{z/\xi}. \quad \text{(A7)}$$

In this model, the evolution is entirely in luminosity; thus, the sources were more luminous in the past if a positive evolution ($k > 0$) is found (the opposite is true otherwise). It is also straightforward to demonstrate that the luminosity evolution peaks at $z_c = -1 - k\xi$.

Finally, we checked the SSRS model (Willott et al. 2001), where the LF is divided into two components:

$$\rho(z, L_\gamma) = (\rho(L_\gamma)_I + \rho(L_\gamma)_{II})\, f(z), \quad \text{(A8)}$$

where

$$\rho(z, L_\gamma)_I = \rho_I^0 \left(\frac{L_\gamma}{L_{Ic}}\right)^{-\alpha_I} \exp\left(-\frac{L_\gamma}{L_{Ic}}\right), \quad \text{(A9)}$$

$$\rho(z, L_\gamma)_{II} = \rho_{II}^0 \left(\frac{L_\gamma}{L_{IIc}}\right)^{-\alpha_{II}} \exp\left(-\frac{L_{IIc}}{L_\gamma}\right), \quad \text{(A10)}$$

and

$$f(z) = \begin{cases} (1+z)^k & \text{if } z \leqslant z_0 \\ (1+z_0)^k & \text{if } z > z_0 \end{cases} \quad \text{(A11)}$$

This model has been used, for instance, by Inoue (2011) and Di Mauro et al. (2014), for the determination of the diffuse $\gamma$-ray emission from misaligned AGNs.

## APPENDIX B

## HSP CATALOG FOR SED DETERMINATION

For completeness, in Table 3 we report the characteristic parameters for the selected HSP BL Lacs, which constitute the class of greatest interest for this work, and where the synergy between HE and VHE observations is more evident: associated name, 2FGL name, redshift, photon index in the range 100 MeV–100 GeV $\Gamma_{\rm HE}$, photon index in the TeV energies $\Gamma_{\rm VHE}$, photon index for $E > 100$ MeV $\Gamma_{\rm cut}$, and energy cutoff $E_{\rm cut}$ found with our analysis for an exponentially cutoff power-law spectrum (see Equation (12)). The values associated with $\Gamma_{\rm HE}$, $\Gamma_{\rm VHE}$, and $z$ are taken from Sanchez et al. (2013) and references therein for all sources except for 1ES 1215+303

(Aleksić et al. 2012), PKS 0447−439 (Perlman et al. 1998; Rovero et al. 2013; Zhou et al. 2013; H.E.S.S. Collaboration et al. 2013b), PG 1553+113 (Danforth et al. 2010; Aharonian et al. 2008), and Mrk 501 (Acciari et al. 2011).

## REFERENCES


Abazajian, K. N., Blanchet, S., & Harding, J. P. 2011, PhRvD, 84, 103007
Abdo, A. A., Ackermann, M., Agudo, I., et al. 2010a, ApJ, 716, 30
Abdo, A. A., Ackermann, M., Ajello, M., et al. 2010b, ApJS, 188, 405
Abdo, A. A., Ackermann, M., Ajello, M., Allafort, A., et al. 2010c, ApJ, 715, 429
Abdo, A. A., Ackermann, M., Ajello, M., et al. 2009, ApJ, 707, 1310
Abdo, A. A., Ackermann, M., Ajello, M., & Fermi LAT Collaboration., 2010d, PhRvL, 104, 101101
Abdo, A. A., Ackermann, M., Ajello, M., & Fermi LAT Collaboration., 2010e, ApJ, 720, 435
Acciari, V. A., Arlen, T., Aune, T., et al. 2011, ApJ, 729, 2
Ackermann, M. 2012, 4th Fermi Symposium, http://galprop.stanford.edu/resources.php
Ackermann, M., Ajello, M., Allafort, A., et al. 2011, ApJ, 743, 171
Ackermann, M., Ajello, M., Allafort, A., et al. 2012a, Sci, 338, 1190
Ackermann, M., Ajello, M., Allafort, A., et al. 2012b, ApJ, 755, 164
Ackermann, M., Ajello, M., Allafort, A., et al. 2012, Sci, 338, 1190
Aharonian, F., Akhperjanian, A. G., Barres de Almeida, U., et al. 2008, A&A, 477, 481
Ajello, M., Romani, R., Gasparrini, D., et al. 2014, ApJ, 780, 73
Ajello, M., Shaw, M. S., Romani, R. W., et al. 2012, ApJ, 751, 108
Aleksić, J., Alvarez, E. A., Antonelli, L. A., et al. 2012, A&A, 544, A142
Angel, J. R. P., & Stockman, H. S. 1980, ARA&A, 18, 321
Begelman, M. C., Rudak, B., & Sikora, M. 1990, ApJ, 362, 38
Boettcher, M. 2012, arXiv:1205.0539
Bringmann, T., Calore, F., Di Mauro, M., & Donato, F. 2013, PRD, 89, 023012
Calore, F., De Romeri, V., & Donato, F. 2012, PhRvD, 85, 023004
Chiang, J., & Mukherjee, R. 1998, ApJ, 496, 752
Danforth, C. W., Keeney, B. A., Stocke, J. T., Shull, J. M., & Yao, Y. 2010, ApJ, 720, 976
Dermer, C. D. 2007, ApJ, 659, 958
Dermer, C. D., Schlickeiser, R., & Mastichiadis, A. 1992, A&A, 256, L27
Di Mauro, M., Calore, F., Donato, F., Ajello, M., & Latronico, L. 2014, ApJ, 780, 161
Doert, M., & Errando, M. 2013, arXiv:1306.6529
Dubus, G., Contreras, J. L., Funk, S., et al. 2013, APh, 43, 317
Essey, W., & Kusenko, A. 2010, APh, 33, 81
Fichtel, C. E., Hartman, R. C., Kniffen, D. A., et al. 1975, ApJ, 198, 163
Finke, J. D., Razzaque, S., & Dermer, C. D. 2010, ApJ, 712, 238
Franceschini, A., Rodighiero, G., & Vaccari, M. 2008, A&A, 487, 837
Ghisellini, G. 1999, ApL&C, 39, 17
Gilmore, R. C., Somerville, R. S., Primack, J. R., & Domínguez, A. 2012, MNRAS, 422, 3189
Hartman, R. C., Bertsch, D. L., Bloom, S. D., et al. 1999, ApJS, 123, 79
Hasinger, G., Miyaji, T., & Schmidt, M. 2005a, A&A, 441, 417
Hasinger, G., Miyaji, T., & Schmidt, M. 2005b, A&A, 441, 417
Henri, G., Pelletier, G., & Roland, J. 1993, ApJL, 404, L41
H.E.S.S. Collaboration, Abramowski, A., Acero, F., et al. 2013a, A&A, 550, A4
H.E.S.S. Collaboration, Abramowski, A., Acero, F., et al. 2013b, A&A, 552, A118
Hogg, D. W. 1999, astro-ph/9905116
Inoue, Y. 2011, ApJ, 733, 66
Inoue, Y., & Ioka, K. 2012, PhRvD, 86, 023003
Inoue, Y., Kalashev, O. E., & Kusenko, A. 2013,
Inoue, Y., & Totani, T. 2009, ApJ, 702, 523
Kalashev, O. E., Semikoz, D. V., & Sigl, G. 2009, PhRvD, 79, 063005
Kneiske, T. M., & Mannheim, K. 2007, A&A, 479, 41
Kraushaar, W. L., Clark, G. W., Garmire, G. P., et al. 1972, ApJ, 177, 341
Mücke, A., & Pohl, M. 2000, MNRAS, 312, 177
Murase, K., Dermer, C. D., Takami, H., & Migliori, G. 2012, ApJ, 749, 63
Narumoto, T., & Totani, T. 2006, ApJ, 643, 81
Neronov, A., & Semikoz, D. 2012, ApJ, 757, 61
Nolan, P. L., Abdo, A. A., Ackermann, M., et al. 2012, ApJS, 199, 31
Padovani, P., & Giommi, P. 1995, ApJ, 444, 567
Perlman, E. S., Padovani, P., Giommi, P., et al. 1998, AJ, 115, 1253
Prandini, E., Bonnoli, G., & Tavecchio, F. 2012, A&A, 543, A111
Prosekin, A., Essey, W., Kusenko, A., & Aharonian, F. 2012, ApJ, 757, 183
Reimer, A., & Böttcher, M. 2013, APh, 43, 103
Rovero, A. C., Donzelli, C., Muriel, H., Cillis, A., & Pichel, A. 2013, arXiv:1307.6907
Sanchez, D. A., Fegan, S., & Giebels, B. 2013, A&A, 554, A75
Schlickeiser, R. 2003, A&A, 410, 397
Sentürk, G., Errando, M., Bttcher, M., & Mukherjee, R. 2013, ApJ, 764, 119
Shaw, M. S., Romani, R. W., Cotter, G., et al. 2012, ApJ, 748, 49
Sreekumar, P., Bertsch, D. L., Dingus, B. L., et al. 1998, ApJ, 494, 523
Stecker, F. W., & Salamon, M. H. 1996, ApJ, 464, 600
Stecker, F. W., & Venters, T. M. 2011, ApJ, 736, 40
The Fermi-LAT Collaboration. 2013, arXiv:1306.6772
Ueda, Y., Akiyama, M., Ohta, K., & Miyaji, T. 2003, ApJ, 598, 886
Urry, C. M., & Padovani, P. 1995, PASP, 107, 803
Venters, T. M., Pavlidou, V., & Reyes, L. C. 2009, ApJ, 703, 1939
Wakely, S., & Deirdre, H. 2013, http://tevcat.uchicago.edu
Willott, C. J., Rawlings, S., Blundell, K. M., Lacy, M., & Eales, S. A. 2001, MNRAS, 322, 536
Yan, D., Zeng, H., & Zhang, L. 2012, MNRAS, 422, 1779
Zeng, H. D., Yan, D. H., Sun, Y. Q., & Zhang, L. 2012, ApJ, 749, 151
Zheng, Y., & Kang, T. 2013, ApJ, 764, 113
Zhou, Y., Yan, D., Dai, B., & Zhang, L. 2013, arXiv:1309.2386